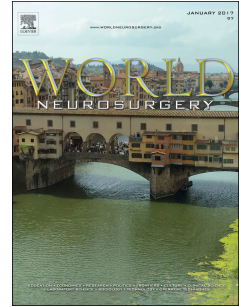


Journal Pre-proof

Differentiating giant cell glioblastoma from classic glioblastoma with diffusion-weighted imaging

Caiqiang Xue, Bin Zhang, Juan Deng, Xianwang Liu, Shenglin Li, Junlin Zhou



PII: S1878-8750(20)32327-5

DOI: <https://doi.org/10.1016/j.wneu.2020.10.125>

Reference: WNEU 16223

To appear in: *World Neurosurgery*

Received Date: 12 September 2020

Revised Date: 21 October 2020

Accepted Date: 22 October 2020

Please cite this article as: Xue C, Zhang B, Deng J, Liu X, Li S, Zhou J, Differentiating giant cell glioblastoma from classic glioblastoma with diffusion-weighted imaging, *World Neurosurgery* (2020), doi: <https://doi.org/10.1016/j.wneu.2020.10.125>.

This is a PDF file of an article that has undergone enhancements after acceptance, such as the addition of a cover page and metadata, and formatting for readability, but it is not yet the definitive version of record. This version will undergo additional copyediting, typesetting and review before it is published in its final form, but we are providing this version to give early visibility of the article. Please note that, during the production process, errors may be discovered which could affect the content, and all legal disclaimers that apply to the journal pertain.

© 2020 Elsevier Inc. All rights reserved.

Credit Author Statement

Caiqiang Xue: Conceptualization, Methodology, Writing- Original draft preparation.

Bin Zhang: Investigation, Data Curation.

Juan Deng: Validation.

Xianwang Liu: Formal analysis.

Shenglin Li: Writing- Reviewing and Editing.

Junlin Zhou: Resources, Visualization, Project administration, Funding acquisition.

Differentiating giant cell glioblastoma from classic glioblastoma with diffusion-weighted imaging

Caiqiang Xue^a, Bin Zhang^a, Juan Deng^a, Xianwang Liu^a, Shenglin Li^a, Junlin Zhou^{a,*}

^a Department of Radiology, Lanzhou University Second Hospital, Second Clinical School, Lanzhou University, Key Laboratory of Medical Imaging of Gansu Province, Lanzhou, Gansu, China

Correspondence: Junlin Zhou, Ph.D., Department of Radiology, Lanzhou University Second Hospital, Cuiyingmen No. 82, Chengguan District, Lanzhou, 730030, PR China.

Email: lzuzjl601@163.com

Funding Sources:

Project type: Lanzhou University Second Hospital “Cuiying Technology Innovation Plan” Applied Basic Research Project

Project name: Expression and prognosis of glioblastoma IDH and MGMT based on radiomics

Item Number: CY2017-MS03

Informed consent

The requirement for informed consent by the study participants was waived due to the retrospective study design.

Author contribution statements

Caiqiang Xue and Bin Zhang equally contributed to this work.

Abstract

Purpose: Differential diagnosis of giant cell glioblastoma (GC) and classic glioblastoma (GBM) using conventional radiological modalities is difficult. This study aimed to use diffusion-weighted imaging (DWI) to distinguish GC from GBM and thereby improve the accuracy of preoperative assessment of patients with GB.

Materials and Methods: The clinical, magnetic resonance imaging, and pathological data of 12 patients with GC and 21 patients with GBM were retrospectively analyzed. Independent sample t-tests were used to compare the minimum apparent diffusion coefficient (ADC_{min}) and the normalized apparent diffusion coefficients (nADC) of the two tumor types. Receiver operating curve (ROC) analysis was used to assess the diagnostic efficacy of ADC_{min} and nADC values.

Results: Compared with that of the classic GBM group, the ADC_{min} (0.98 ± 0.14 vs. $0.80 \pm 0.19 \times 10^{-3} \text{ mm}^2/\text{s}$, $P = 0.007$) and nADC (1.42 ± 0.25 vs. 1.17 ± 0.25 , $P=0.011$) of the GC group were significantly higher. ROC curve analysis showed that, the maximum AUC of ADC_{min} and nADC were 0.800 ± 0.080 and 0.778 ± 0.082 , respectively. The sensitivity, specificity and accuracy distinguishing GC and classic GBM was best (83.33%, 76.19%, and 78.79%, respectively) when $ADC_{min}=0.84 \times 10^{-3} \text{ mm}^2/\text{s}$ (maximum area under the ROC, 0.800). Its positive and negative predictive values under this condition were 88.89% and 66.67%, respectively.

Conclusion: By distinguishing GC from classic GBM, the ADC_{min} parameter of DWI can improve the accuracy of the preoperative differential diagnosis of the two tumor types.

Keywords: Giant cell; Glioblastoma; Magnetic resonance imaging; Diffusion-weighted imaging; Apparent diffusion coefficient

Giant cell glioblastoma (GC) are composed of large cells with polymorphic nuclei, eosinophilic cytoplasm, and increased reticular fibers¹; furthermore, GCs are characterized by rare vascular endothelial cell proliferation. Accounting for 2–5% of all glioblastoma (GBM) cases, GC primarily presents in the temporal lobes of younger men^{2,3}. Although GC is a special subtype of GBM with similar clinical signs and symptoms, the prognosis of GC is better than that of classic GBM. Furthermore, prolonged survival (i.e., 5 years) is rare for GBM patients, whereas it is observed in more than 10% of GC patients (overall 5-year survival: GC, 12.3%; GBM, 3.4%)⁴. Compared with GBM, the boundaries of GC are clearer, and it is easier to completely resect the former with surgery⁵. Hence, maximal surgical resection combined with active adjuvant chemoradiation improves the prognosis of patients with GC^{2,6}. The accurate preoperative diagnosis of GC is vital to the success of personalized clinical treatment.

As a functional magnetic resonance imaging (MRI) method, diffusion-weighted imaging (DWI) can be used to quantify the diffusion of water molecules along the diffusion gradient in the tissue, which depends on the cell density and membrane integrity: the higher the cell density, the stronger the DWI signal^{7,8}. At present, DWI and ADC values are widely used in the classification, molecular typing, and prediction of the aggressiveness of various tumors. Using the normalized apparent diffusion coefficient (nADC) to grade nonfunctional pancreatic neuroendocrine tumors, Kulali et al. found that the nADC value of high-level nonfunctional pancreatic neuroendocrine tumors was lower than those the values in medium- and low-level counterparts⁹. Xing et al. found that the ADC_{min} and nADC values of isocitrate dehydrogenase (IDH) mutant grade II and grade III astrocytoma were significantly higher than those of the IDH wild-type; the group further found that combining conventional MRI and dynamic susceptibility-contrast perfusion-weighted imaging to predict the IDH mutation status of grade II and III astrocytoma had a high sensitivity, specificity, and positive and negative predictive values¹⁰. Song et al. used ADC values to predict the invasiveness of papillary thyroid carcinoma and found that ADC_{min} can provide quantitative information to distinguish low-invasive from high-invasive PTC lesions¹¹. However, GC and classic GBM appear similarly on conventional MRI and can thus be difficult to distinguish. This study aimed to use the ADC value to inform the preoperative differential diagnosis of GC and classic GBM to improve the accuracy of diagnosing and treating either type of glioblastoma.

Materials and Methods

The present study was approved by the local institutional review board and the need for informed consent was waived due to the retrospective study design.

Patients

The clinical, pathological, and imaging data of 12 and 21 randomly selected patients who were treated for GC and classic GBM, respectively, from May 2015 to May 2020 were collected. The diagnoses of GC and GBM were confirmed by surgery

years). The mean age of the patients with GB was 52.5 ± 12.8 years (age range, 31–71 years). Clinical manifestations included 28 cases of headache and dizziness, three cases of dysfunction or limb paralysis, one case of slurred speech, and one case of other manifestations.

MRI protocol

Head MRI and enhanced scanning were performed with a Siemens Verio 3.0 T superconducting MRI scanner while the patients were in the supine position. Scanning parameters were set to the following: T1-weighted imaging (T1WI) (gradient echo sequence): TR, 550 ms; TE, 11 ms; layer thickness, 5.0 mm; layer interval, 1.5 mm; field of view (FOV), $260 \text{ mm} \times 260 \text{ mm}$; matrix size, 256×256 ; T2WI (turbo spin-echo sequence): TR, 2200 ms; TE, 96 ms; echo time, 10 ms; echo chain length, 8; excitation number, 2; DWI (spin-echo echo-planar imaging sequence): frequency-selective fat suppression technology (retention time [TR], 4000 ms); echo time (TE), 100 ms; layer thickness, 5 mm; layer spacing, 1.5 mm; FOV, $260 \text{ mm} \times 260 \text{ mm}$; matrix size, 256×256 . The two b values of 0 and 1000 s/mm were used in three orthogonal directions. We used Gd-DTPA ([Bayer Schering Pharma AG, Berlin, Germany]/kg) as the enhanced scanning contrast agent, which was intravenously administered via a bolus injection of 0.1 mmol/kg at a flow rate of 3.0 ml/s.

MRI image evaluation

Two neuroradiologists with more than 10 years of diagnostic experience independently and blindly analyzed the MRI images of each patient. The tumor number, location, maximum diameter, necrosis/cystic changes, edema around the tumor, tumor boundary, and enhancement method were recorded. After the DWI scan was completed, the corresponding ADC image was obtained with a computer post-processing algorithm according to the original DWI image. The ADC image was then transmitted to the Siemens post-processor to measure the ADC of the solid part of the tumor. The solid part of the tumor was selected on multiple consecutive ADC maps, and the six to eight regions of interest (ROI) with an area of $15\text{--}20 \text{ mm}^2$ were manually placed on each level. The area with the lowest ADC value (ADC_{\min}) was selected. The averages of the minimum ADC values calculated by the two radiologists were used as the final result. The ADC of normal white matter (NAWM) was measured from the center of both half eggs. In patients with tumors or related angioedema involving the side of the semi-oval, the ADC was calculated only from the side of the center of the semi-oval. Free-form marking tools were used to manually draw tumor contour image slices on the ADC map of each ADC, and the mean ADC (ADC_{mean}) was calculated. The normalized ADC (nADC) was obtained by dividing the ADC_{mean} by the average NAWM value.

Statistical analysis

All data were analyzed with SPSS 25.0 statistical software. A chi-square test was used to compare the tumor count variables

calculated by the two radiologists. ICC values of greater than 0.75 indicated excellent consistency. Two sample t-tests were performed to compare the patient's age, tumor size, ADC_{min} , and nADC. P-values of <0.05 were considered to indicate statistical significance. The ROC curve was used to assess the differential diagnosis ability of ADC_{min} and nADC.

Results

The GC and GBM groups featured similar sex distributions (eight men and four women vs. 13 men and eight women, $P=1.00$). In addition, the average ages of the patients with GC and classic GBM were also similar (51.3 ± 11.7 vs. 52.5 ± 12.8 years, $P=0.79$). Six of the GCs were located in the temporal lobe, one in the frontal lobe, one in the cerebellar hemisphere, two in the occipital lobe, and two in the parietal lobe. Seven of the classic GBMs were situated in the temporal lobe, four in the frontal lobe, six in the parietal lobe, and four in the occipital lobe. There were no statistically significant differences between the distribution of the GCs and classic GBMs in the temporal lobe ($P=0.47$).

Conventional MRI revealed the maximum diameter of the GCs to be 7.6 cm (average, 5.08 ± 2.09 cm; range, 1.2–7.6 cm) and that of the classic GBMs to be 8.7 cm (average, 5.40 ± 1.24 cm; range, 3.1–8.7 cm), indicating that the tumor sizes in both groups were similar ($P>0.05$). No significant differences in the conventional MRI parameters of GCs and classic GBMs were found (Table 1). Typical GC and classic GBM images are shown in Figures 1 and 2. The ADC_{min} and nADC of the GC and GBM groups are shown in Table 2. The solid parts of nine GCs showed high-signal intensities on DWI, those of two showed equal signals, and that of one showed low signal. The solid parts of 17 classic GBMs showed high-signal intensities on DWI, those of two showed equal signal, and that of one showed low signal. The agreement between the ADC parameters calculated by the two observers was excellent: the ICCs of ADC_{min} and nADC were 0.83 and 0.79, respectively. In addition, compared with GBM group, the GC group featured significantly higher ADC_{min} (0.98 ± 0.14 vs. $0.80 \pm 0.19 \times 10^{-3} \text{ mm}^2/\text{s}$, $P = 0.007$) and nADC (1.42 ± 0.25 vs. 1.17 ± 0.25 , $P=0.011$). ROC curve analysis showed that, when distinguishing GC from classic GBM, the maximum AUC of ADC_{min} and nADC were 0.800 ± 0.080 and 0.778 ± 0.082 , respectively (Table 3, Figure 3). When ADC_{min} was $0.84 \times 10^{-3} \text{ mm}^2/\text{s}$, the sensitivity, specificity, and accuracy reached their maximum values of 83.33%, 76.19%, and 78.79%, respectively; the positive and negative predictive values under this condition were 88.89% and 66.67%, respectively.

Discussion

This retrospective study aimed to evaluate the ability of DWI to overcome the difficulty in differentially diagnosing GC and classic GBM with conventional MRI. We found the ADC_{min} and nADC DWI parameters of the two tumors to be significantly different and can thus be used to distinguishing them.

The 2016 World Health Organization (WHO) Central System Tumor Classification classified glioblastoma as a WHO IV tumor that originates from astrocytes and is characterized by high invasiveness and recurrence rate¹². Patients with GC

^{13, 14}. Before adopting a chemotherapy regimen, however, it is necessary to fully evaluate the prognostic implications of GC. As GC clinical symptoms are atypical and it can be difficult to distinguish GC from GBM with conventional MRI, DWI examination should be used to distinguish GC from classic GBM and inform appropriate patient management or treatment planning before performing a biopsy.

Concerning the clinical similarities between GC and GBM that complicate their differential diagnosis, the features of GC overlap with those of GBM. While the age of GC onset is reportedly younger than that of GBM onset ¹⁵; our study did not identify a significant difference between the two (51.3 ± 11.7 vs. 52.5 ± 12.8 years; $P=0.79$). There is also no significant statistical difference between the two group ($P>0.05$). The literature reports that GC more commonly presents in the temporal lobe than does GBM¹⁵. Of the 12 GCs considered in the present study, six occurred in the temporal lobe (50.00%), while seven of the 21 GBMs were observed in the temporal lobe (29.17%). However, we found that the distribution of the GCs in the temporal lobe did not differ statistically that of the classical GBM ($P>0.05$). This finding is consistent with those of a previous report ⁴. In addition, no signs on conventional MRI were found to be reliably capable of distinguishing GC from classic GBM.

Research has confirmed that the ADC value obtainable with DWI can be used to grade gliomas: the lower the ADC value, the higher the grade ¹⁶. Daniel et al. found that ADC histograms can classify low-grade astrocytoma, oligodendroglioma, and oligodendro-astrocytoma, and that the accuracy of distinguishing astrocytoma from oligodendroglioma could reach 83% ¹⁷. We found that the ADC_{min} and nADC of GC to be significantly higher than those of classic GBM. We further found that the sensitivity, specificity, and accuracy of distinguishing GC from classic GBM were the best (83.33%, 76.19%, and 78.79%, respectively) when ADC_{min} reached $0.84 \times 10^{-3} \text{ mm}^2/\text{s}$.

Since the diffusion of water in tissues is highly dependent on the ratio of intracellular to extracellular space, the higher cell density in advanced tumors reduces the diffusion of water molecules by limiting the available extracellular space ⁸. GBM is pathologically characterized by increased mitotic activity, increased heterogeneity, and an increased number of cells ¹⁸. In contrast, GC cells are bulky, have atypically shaped nuclei, are very basophilic, and have increased reticular fibers ^{1, 5}. The ADC values of gliomas are significantly negatively correlated with cell density: the greater the cell density, the smaller the ADC value ¹⁹. We consider that the differences in these structural features may account for the relatively large ADC_{min} and nADC values of GC. As ADC values reportedly decrease as malignancy increases ²⁰, the presently identified difference in ADC values between GC and classic GBM verify the lower malignancy of GC. Research has confirmed that low ADC values were factors for a poor prognosis in gliomas ²¹. In our study, the ADC_{min} and nADC values of GC were significantly higher than GBM, and the prognosis of GC was better than GBM. It indicates that ADC_{min} and nADC values are related to the prognosis of GC and GBM. The prognosis of both can be evaluated by ADC value before surgery.

The study was subject to the limitation of small sample sizes that may have caused statistical bias. Further, selection bias may have been introduced by our having measured the ROI in the solid parts of the tumor rather than considering the entire

Conclusions

DWI combined with ADC can distinguish GC from classic GBM and may be used as a non-invasive bio-imaging marker for GBM subtype classification.

Journal Pre-proof

1. Ogawa K, Kurose A, Kamataki A, Asano K, Katayama K, Kurotaki H. Giant cell glioblastoma is a distinctive subtype of glioma characterized by vulnerability to DNA damage. *Brain tumor pathology*. 2020;37(1): 5-13. <https://doi.org/10.1007/s10014-019-00355-w>.
2. Margetts JC, Kalyan-Raman UP. Giant-celled glioblastoma of brain. A clinico-pathological and radiological study of ten cases (including immunohistochemistry and ultrastructure). *Cancer*. 1989;63(3): 524-531. [https://doi.org/10.1002/1097-0142\(19890201\)63:3<524::aid-cnrcr2820630321>3.0.co;2-d](https://doi.org/10.1002/1097-0142(19890201)63:3<524::aid-cnrcr2820630321>3.0.co;2-d).
3. Katoh M, Aida T, Sugimoto S, et al. Immunohistochemical analysis of giant cell glioblastoma. *Pathology international*. 1995;45(4): 275-282. <https://doi.org/10.1111/j.1440-1827.1995.tb03456.x>.
4. Kozak KR, Moody JS. Giant cell glioblastoma: a glioblastoma subtype with distinct epidemiology and superior prognosis. *Neuro-oncology*. 2009;11(6): 833-841. <https://doi.org/10.1215/15228517-2008-123>.
5. Sabel M, Reifenberger J, Weber RG, Reifenberger G, Schmitt HP. Long-term survival of a patient with giant cell glioblastoma. Case report. *J Neurosurg*. 2001;94(4): 605-611. <https://doi.org/10.3171/jns.2001.94.4.0605>.
6. Bauchet L, Mathieu-Daudé H, Fabbro-Peray P, et al. Oncological patterns of care and outcome for 952 patients with newly diagnosed glioblastoma in 2004. *Neuro-oncology*. 2010;12(7): 725-735. <https://doi.org/10.1093/neuonc/noq030>.
7. Waseda Y, Yoshida S, Takahara T, et al. Utility of computed diffusion-weighted MRI for predicting aggressiveness of prostate cancer. *Journal of magnetic resonance imaging : JMRI*. 2017;46(2): 490-496. <https://doi.org/10.1002/jmri.25593>.
8. Xiaoi K, Qing Z, Lei H, Junlin Z. Differentiating microcystic meningioma from atypical meningioma using diffusion-weighted imaging. *Neuroradiology*. 2020;62(5): 601-607. <https://doi.org/10.1007/s00234-020-02374-3>.
9. Kulali F, Semiz-Oysu A, Demir M, Segmen-Yilmaz M, Bukte Y. Role of diffusion-weighted MR imaging in predicting the grade of nonfunctional pancreatic neuroendocrine tumors. *Diagnostic and interventional imaging*. 2018;99(5): 301-309. <https://doi.org/10.1016/j.diii.2017.10.012>.
10. Xing Z, Yang X, She D, Lin Y, Zhang Y, Cao D. Noninvasive Assessment of IDH Mutational Status in World Health Organization Grade II and III Astrocytomas Using DWI and DSC-PWI Combined with Conventional MR Imaging. *AJNR American journal of neuroradiology*. 2017;38(6): 1138-1144. <https://doi.org/10.3174/ajnr.A5171>.
11. Song B, Wang H, Chen Y, Liu W, Wei R, Ding Y. Efficacy of apparent diffusion coefficient in predicting aggressive histological features of papillary thyroid carcinoma. *Diagnostic and interventional radiology (Ankara, Turkey)*. 2018;24(6): 348-356. <https://doi.org/10.5152/dir.2018.18130>.
12. Louis DN, Perry A, Reifenberger G, et al. The 2016 World Health Organization Classification of Tumors of the Central Nervous System: a summary. *Acta neuropathologica*. 2016;131(6): 803-820. <https://doi.org/10.1007/s00401-016-1545-1>.
13. Oh T, Rutkowski MJ, Safaee M, et al. Survival outcomes of giant cell glioblastoma: institutional experience in the management of 20 patients. *Journal of clinical neuroscience : official journal of the Neurosurgical Society of Australasia*. 2014;21(12): 2129-2134. <https://doi.org/10.1016/j.jocn.2014.04.011>.
14. Temme A, Geiger KD, Wiedemuth R, et al. Giant cell glioblastoma is associated with altered aurora b expression and concomitant p53 mutation. *Journal of neuropathology and experimental neurology*. 2010;69(6): 632-642. <https://doi.org/10.1097/NEN.0b013e3181e4c06e>.
15. De Prada I, Cordobés F, Azorín D, Contra T, Colmenero I, Glez-Mediero I. Pediatric giant cell glioblastoma: a case report and review of the literature. *Child's nervous system : ChNS : official journal of the International Society for Pediatric Neurosurgery*. 2006;22(3): 285-289. <https://doi.org/10.1007/s00381-005-1178-5>.
16. Yamasaki F, Kurisu K, Satoh K, et al. Apparent diffusion coefficient of human brain tumors at MR imaging. *Radiology*. 2005;235(3): 985-991. <https://doi.org/10.1148/radiol.2353031338>.
17. Tozer DJ, Jäger HR, Danchaivijitr N, et al. Apparent diffusion coefficient histograms may predict low-grade glioma subtype. *NMR in biomedicine*. 2007;20(1): 49-57. <https://doi.org/10.1002/nbm.1091>.
18. Aldape K, Zadeh G, Mansouri S, Reifenberger G, von Deimling A. Glioblastoma: pathology, molecular mechanisms and markers. *Acta neuropathologica*. 2015;129(6): 829-848. <https://doi.org/10.1007/s00401-015-1432-1>.
19. Gupta RK, Cloughesy TF, Sinha U, et al. Relationships between choline magnetic resonance spectroscopy, apparent diffusion coefficient and quantitative histopathology in human glioma. *Journal of neuro-oncology*. 2000;50(3): 215-226. <https://doi.org/10.1023/a:1006431120031>.

21. Zeng Q, Dong F, Shi F, Ling C, Jiang B, Zhang J. Apparent diffusion coefficient maps obtained from high b value diffusion-weighted imaging in the preoperative evaluation of gliomas at 3T: comparison with standard b value diffusion-weighted imaging. *Eur Radiol*. 2017;27(12): 5309-5315. <https://doi.org/10.1007/s00330-017-4910-0>.

6. Figure Legends

Figure 1 Female, 36 years old, giant cell glioblastoma of the right occipital lobe. A-C: Magnetic resonance imaging cross-sections. T1-weighted imaging, T2-weighted imaging, and enhanced T1-weighted imaging show a right-sided parietal subcortical-like circular footprint with clear boundaries and uneven signals of about 6.0 cm × 4.5 cm × 5.6 cm in size with long T1 and short T2 signals. Flaky high-signal edema bands surround the solid part, which is obviously strengthened unevenly after the enhancement. D-E: Diffusion-weighted imaging. The main body of the lesion showed a low signal, and the apparent diffusion coefficient showed a low signal. F: Pathological image of the tumor. The tumor cells are arranged in high density, the cytoplasm is eosinophilic, the proportion of nucleoplasm is increased, and the nuclear atypia is evident (HE, ×200).

Figure 2 Female patient, 55 years old, giant cell glioblastoma of the left parietal lobe. A-C: Magnetic resonance imaging cross-sections. T1-weighted imaging, T2-weighted imaging, and enhanced T1-weighted imaging show a left subparietal cortex-like circular footprint, with unclear boundaries and uneven signals of about 6.2 cm × 4.4 cm × 5.2 cm in size, with long T1 and long T2 signals. Flaky high-signal edema bands surround the solid part, which is obviously unevenly strengthened. The surrounding subfocals are visible. D-E: Diffusion-weighted imaging. The main body of the lesion showed a slightly higher signal, and the apparent diffusion coefficient showed a slightly lower signal. F: Pathological image of the tumor. The tumor cells are densely hyperplastic, the nucleoplasm ratio is increased, and the nuclear atypia is evident (HE, ×100).

Figure 3 Giant cell glioblastoma and classic glioblastoma. The minimum and normalized apparent diffusion coefficients indicate the differential diagnostic efficiency. The areas under the curve is 0.800 ± 0.080 and 0.778 ± 0.082 , respectively.

Table 1. The demographic data and conventional MRI characteristics of patients with GC and classic GBM

	GC (n=12)	GBM (n=21)	P-value
Age (years)	51.3±11.7	52.5±12.8	0.79
Sex (man/woman)	8/4	13/8	1.00
Location (temporal lobe/other)	6/6	7/14	0.47
Number (single/multiple)	10/2	20/1	0.54
Maximum diameter of tumor (cm)	5.08±2.09	5.40±1.24	0.58
Edema – yes	11 (91.7%)	21 (100%)	0.36
Clear tumor-brain interface	7 (58.3%)	7 (33.3%)	0.27
Cystic change – yes	7 (58.3%)	14 (66.7%)	0.72
Necrosis – yes	10 (83.3%)	20 (95.2%)	0.54
Enhancement method (light-to-moderate/obvious)	2/10	1/20	0.54

Abbreviations: GC, giant cell glioblastoma; GBM, classic glioblastoma

Table 2 Comparison of ADC_{min} value and nADC value between GC and classic GBM

Parameter ($\times 10^{-3}$ mm ² /s)	GC (n=12)	GB (n=21)	P-value
ADC _{min}	0.98 \pm 0.14	0.80 \pm 0.19	< 0.05
nADC	1.42 \pm 0.25	1.18 \pm 0.25	< 0.05

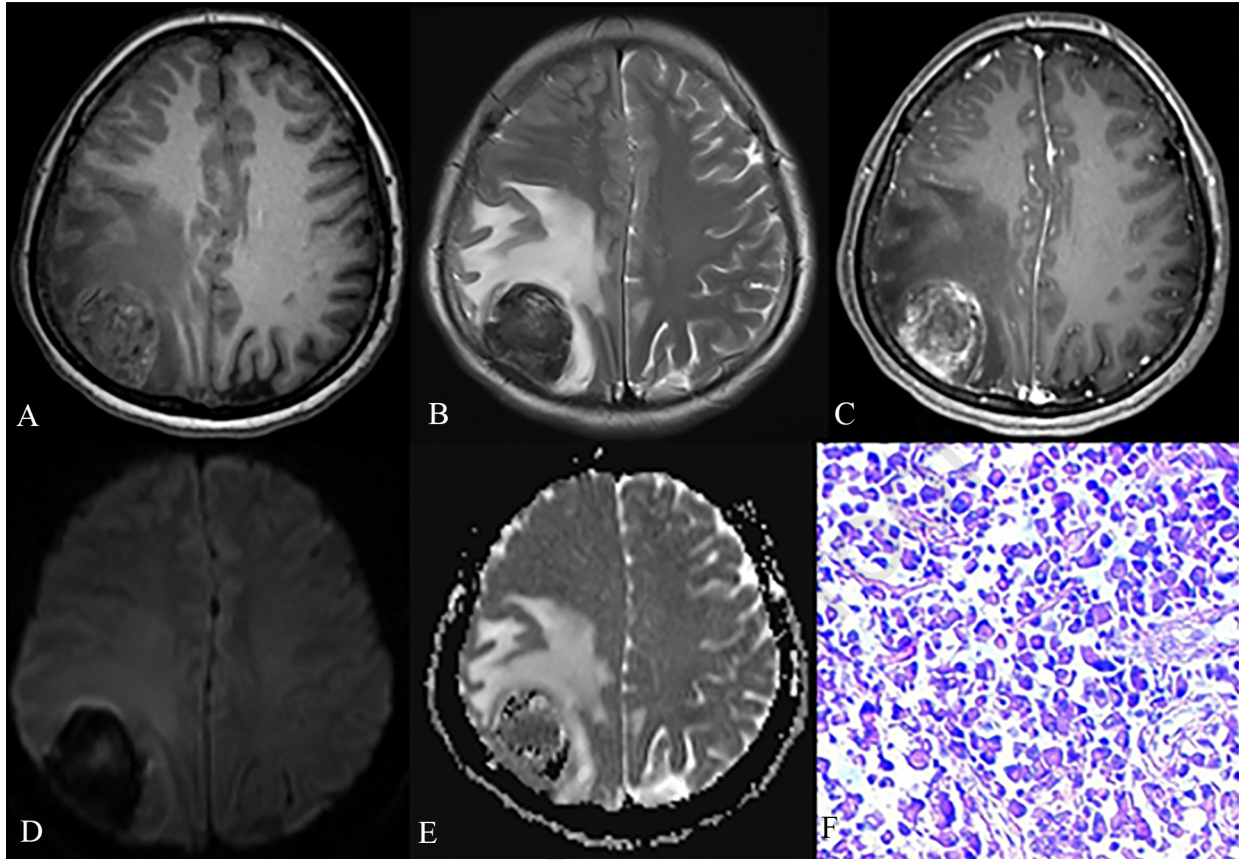
Abbreviations: ADC, apparent dispersion coefficient; ADC_{min}, minimum ADC; nADC, normalized ADC; GC, giant cell glioblastoma; GBM, classic glioblastoma

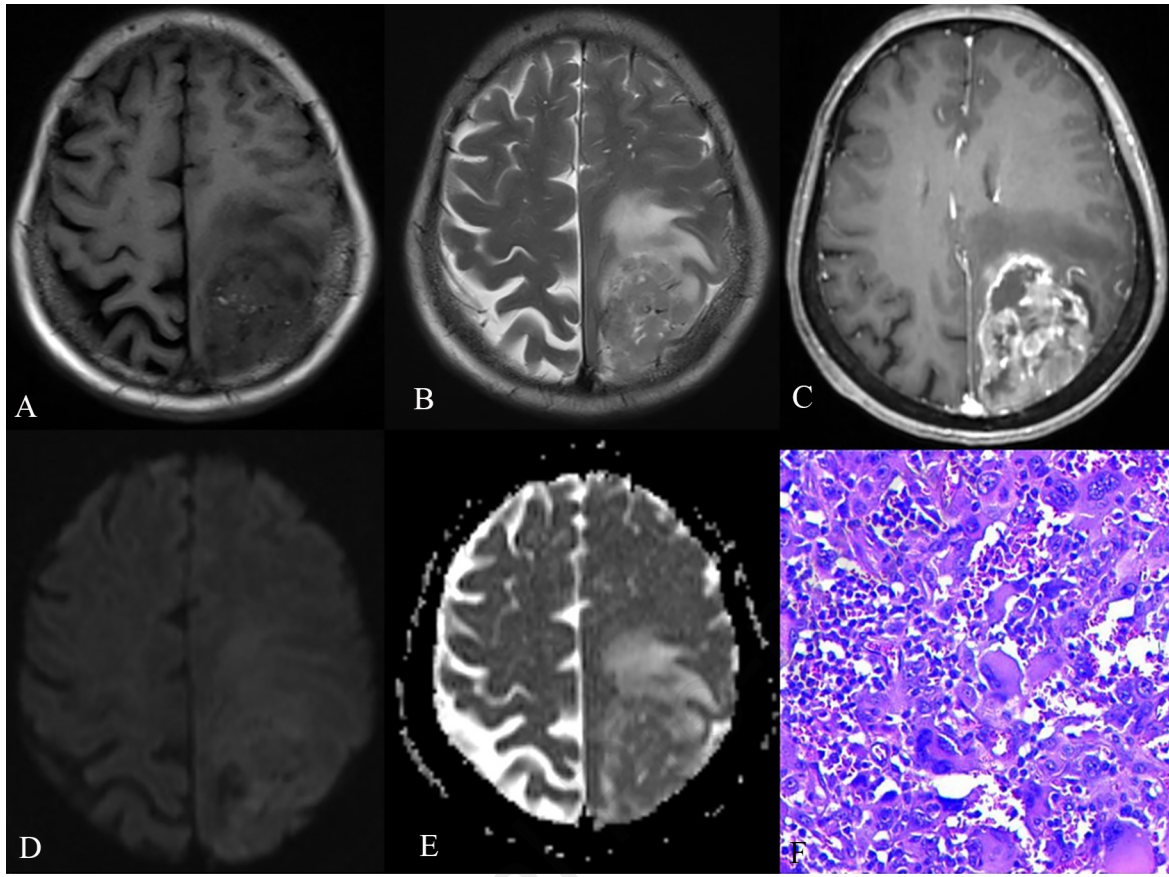
Table 3 Diagnostic performance of ADC parameters for differentiating GC from classic GB

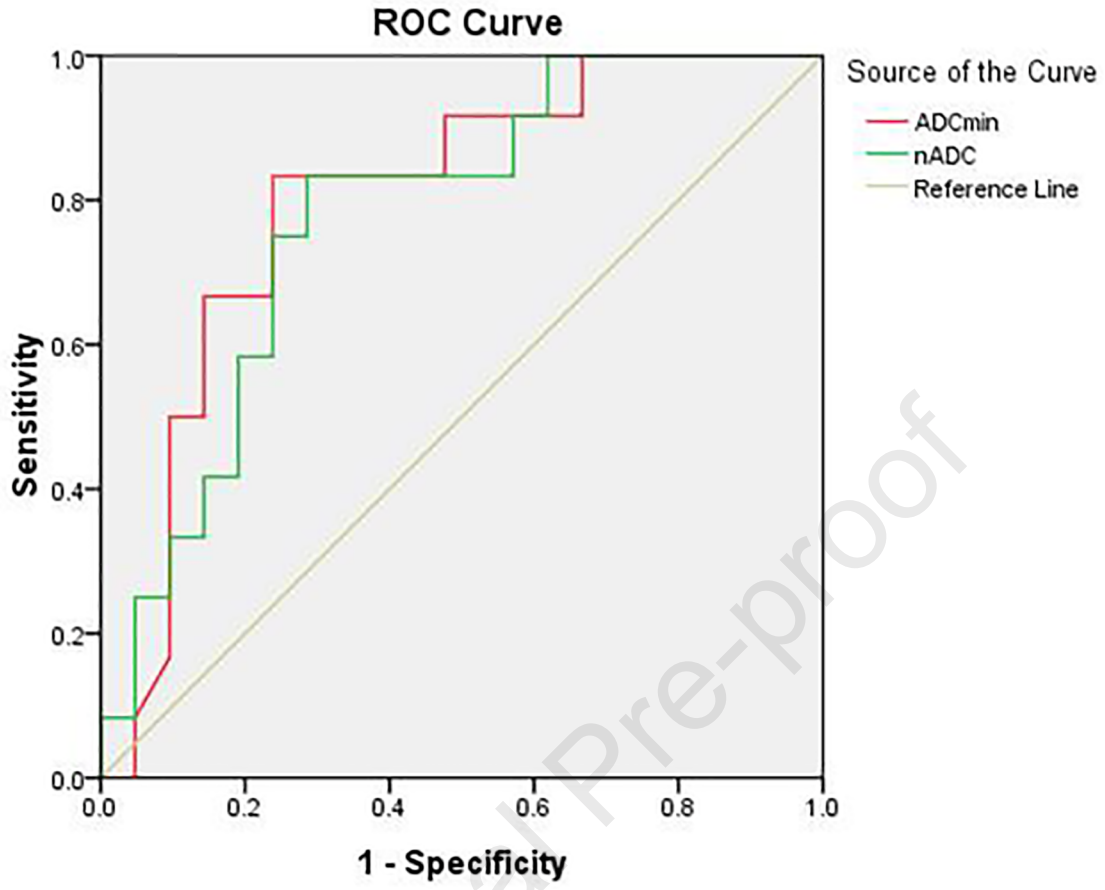
	Cut-off ($\times 10^{-3}$ mm ² /s)	Sen (%)	Sep (%)	PPV (%)	NPV (%)	ACC (%)	AUC
ADC _{min}	0.84	83.33	76.19	88.89	66.67	78.79	0.800
nADC	1.25	83.33	71.43	88.24	62.50	75.76	0.778

Abbreviations: ADC, apparent dispersion coefficient; GC, giant cell glioblastoma; GBM, classic

glioblastoma; ADC_{min}, minimum ADC; nADC, normalized ADC; Sen, Sensitivity; Sep, Specificity; PPV, Positive predictive value; NPV, Negative predictive value; ACC, Accuracy; AUC, Area under curve







Conflict of interest statement:

The authors declare that the article content was composed in the absence of any commercial or financial relationships that could be construed as a potential conflict of interest.

Journal Pre-proof

ADC: Apparent diffusion coefficient
ADC_{min}: minimum apparent diffusion coefficient
nADC: normalized apparent diffusion coefficients
ROC: Receiver operating curve
MRI: magnetic resonance imaging
DWI: Diffusion-weighted magnetic resonance imaging
FLAIR: Fluid-attenuated inversion recovery
FOV: Field of view
GRE: Gradient-recalled echo
GTR: Gross total resection
ICC: Intraclass correlation coefficient
NAWM: Normal-appearing cerebral white matter
P/R: Progression/recurrence
PSPF: Parasagittal and parafalcine
ROI: Region of interest
T1WI: T1-weighted imaging
T2WI: T2-weighted imaging
TR/TE: Repetition time/echo time
WHO: World Health Organization
GC: giant cell glioblastoma
GBM: glioblastoma
IDH: isocitrate dehydrogenase
ICC: intra-class correlation
WHO: World Health Organization